

*promoting access to White Rose research papers*



**Universities of Leeds, Sheffield and York**  
**<http://eprints.whiterose.ac.uk/>**

---

This is an author produced version of a conference paper presented at **UK e-Science All Hands Meeting 2006**

White Rose Research Online URL for this paper:

<http://eprints.whiterose.ac.uk/id/eprint/78060>

---

**Paper:**

Handley, J, Brodlie, KW and Clayton, RH (2006) *Model based visualization of cardiac virtual tissue*. In: Cox, SJ, (ed.) Proceedings of the UK e-Science All Hands Meeting 2006. UK e-Science All Hands Meeting 2006, 18th-21st September 2006, Nottingham, UK. NeSC , 233 - 240. ISBN 0-9553988-0-0

<http://www.allhands.org.uk/2006/>

---

# Model Based Visualization of Cardiac Virtual Tissue

J W Handley\*, K W Brodli\*, R H Clayton†

\* School of Computing, University of Leeds, Leeds LS2 9JT

† University of Sheffield, Department of Computer Science,  
Regent Court, 211 Portobello Street, Sheffield S1 4DP

## Abstract

In standard analysis of simulations of the heart, usually only one state variable – the trans-membrane voltage (or action potential) – is visualized. While this is the ‘most important’ variable to visualize, all but the most basic cardiac models have many state variables at each node; data that are not used when visualizing the output. In this paper, we present a novel visualization technique developed within the Integrative Biology project that uses the entire state of the cardiac virtual tissue to produce images based on the deviation from normal propagation of action potential.

## 1 Introduction

The current generation of high performance computers enable complex simulations of cardiac tissue with anatomically detailed geometries [2, 10] — yet the output of these simulations are usually visualized using a single output from the models; the trans-membrane voltage, or action potential. This leads to images such as those shown in Figure 1 (see also, for example, [8].) In a normal heartbeat the action potential propagates from cell to cell as a plane wave across the tissue (Figure 1 (a)), but this propagation can break down into the circulating pattern of re-entry (Figures 1 (b) and (c)), a potentially lethal malfunction of heart function. Cardiac arrhythmias such as this are an important cause of premature death in the industrialised world, yet the mechanisms that initiate and sustain the lethal arrhythmias of ventricular fibrillation (VF) and ventricular tachycardia (VT) remain poorly understood.

Experimental and clinical studies of VF mechanisms are limited because it is difficult to record electrical activity throughout the 3D ventricular wall, and so most studies are limited to surface recordings — membrane voltage can be imaged on the surface of experimental preparations of heart tissue using voltage sensitive fluorescent dyes. Computational

models, however, allow us to examine the whole tissue, and models of action potential propagation in cardiac tissue (cardiac virtual tissues - CVT) have been used extensively in the last decade to probe the mechanisms of VF [7].

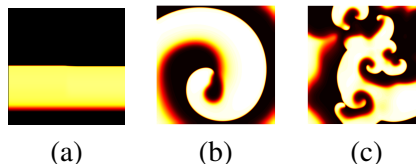


**Figure 1: Example visualizations of 2D cardiac virtual tissues with (a) normal propagation, and re-entrant propagation with (b) one and (c) many re-entrant waves visualized using a colourmap where large values are represented by brighter colours.**

The action potential is the most important state variable in the models to visualize — the action potential propagates from cell to cell, and acts as a signal for cardiac tissue to contract, i.e. it causes the heart to beat. However, the propagation of the action potential is modulated by the conductance of ion channels in the cell membrane. Slowing or blocking of the action potential can result in re-entry, and so the contribution of these ion channels is important. These cannot be imaged in experimen-

tal preparations, but are available in computational models via state variables. Including these variables in visualizations should provide insight into abnormal cardiac function, such as arrhythmias. In this paper we discuss the issues of visualizing *all* the state variables, and present a technique for doing so.

## 2 Visualizing Cardiac Virtual Tissue

In the CVT used throughout this paper, action potential propagation is modelled by a reaction diffusion partial differential equation [1]. Several different excitation models can be used, and these range from simplified models with 3 or 4 state variables, to more detailed models with large nonlinear, stiff systems of ODEs and tens of state variables [6]. The equations are solved across a grid, and typical grid geometries are a 2D sheet, a 3D slab, or an anatomically detailed representation of the heart ventricles.

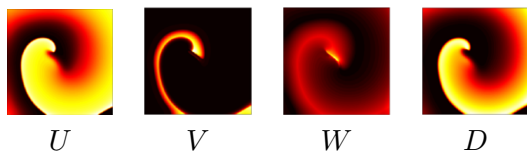


**Figure 2:** A snapshot of re-entry in a 2D model with excitation described by the 4 variable Fenton Karma model [4]. The four state variables are shown individually using the ‘hot’ colourmap where low brightness corresponds to low values.

The visualization challenge can be grasped very quickly through looking at the outputs of two different 2D cardiac virtual tissues. Figure 2 shows a snapshot of the state of a 2D CVT in which a re-entrant wave is rotating. In this model excitability is simulated with the simplified 4 variable Fenton Karma model [4] and in this visualization each state variable is visualized separately. Figure 3 shows a similar snapshot of a re-entrant wave in a CVT where excitability is modelled using a modification of the biophysically detailed Luo Rudy

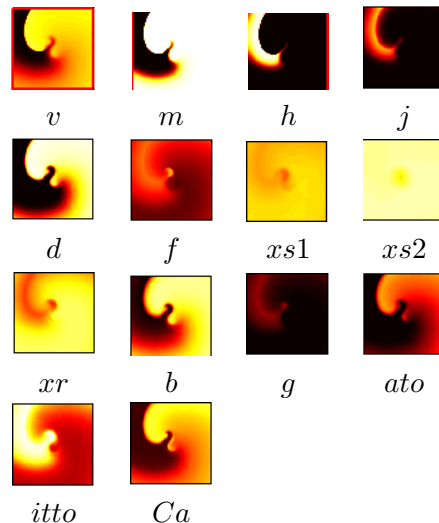


**Figure 3:** Snapshot of re-entry in a 2D model with excitation described by the biophysically detailed Luo Rudy 2 model [3]. As with Figure 2, each state variable is shown individually, except in this model there are 14 state variables.

2 model [3], which has 14 state variables. It is much more difficult to assimilate the 14 images of Figure 3 into a single mental model of the state of the simulation than the four images of Figure 2.

There are many existing techniques for visualizing multi-variate data, such as parallel coordinates, iconic representations or ‘glyphs’, and a review of these and other approaches to the visualization of complex data can be found in [9], however none of these techniques successfully handle data that are, and need to remain, four dimensional (i.e. three spatial dimensions and one temporal) while also being (highly) multi-variate. In this paper, therefore, we concentrate on attempting to reduce the data to a uni-variate space, which can then be visualized easily in four dimensions (using animations of isosurfaces, volume rendering, and so on).

Fortunately the dozens of state variables in CVT are not entirely independent, which makes the visualization process easier. This interdependence has two main impacts;

1. Not every state variable will contribute extra information, and some therefore

may be left out of the visualization, and

2. A collection of state variables can be collapsed into a single ‘meta-variable’ which represents the value of all its constituent variables. For example, the parameters  $m, h$ , and  $j$  in Figure 3 all depend on membrane voltage and time, and determine the magnitude of current through the  $\text{Na}^+$  channel in the cell membrane, which is needed for an action potential to propagate.

The first point can be seen if the correlation co-efficient is calculated between each pair of variables in the four variable Fenton Karma model at each point in time. The correlation used every pixel in a pairwise fashion between each pair of state variables, and can be seen in Figure 4. Note that  $U$  and  $D$  are almost perfectly correlated across the whole simulation, which suggests there would be little extra information gained through including both of these variables in a visualization.

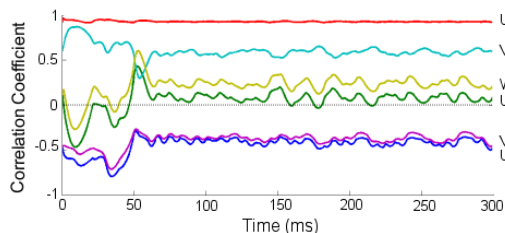


**Figure 4:** The correlation coefficients of each pair of state variables in the Fenton Karma four variable model across an entire simulation. The two letters at the right-hand end of each trace indicate which pair the correlation refers to.

In this paper, we focus on forming visualizations based on every state variable, with the approaches above highlighted as a future refinement.

### 3 Visualizing in Phase Space

The nature of the propagation of action potential through the heart imposes a structure of sorts on the data, as each cell goes through a

cycle of excitation and recovery. This structure becomes apparent, at least with more simple models, when the data is visualized in phase space. In the case of a tri-variate model, if the standard visualization at time  $t$  is to generate three  $n$  by  $m$  pixel images  $U_t(x, y)$ ,  $V_t(x, y)$ , and  $W_t(x, y)$ , for  $0 < x < n$  and  $0 < y < m$ , the phase space visualization is a single 3D scatter-plot image obtained by plotting  $n \times m$  ‘dots’, one at each  $(U_t(x, y), V_t(x, y), W_t(x, y))$ . Figure 5 shows examples of phase space plots from a Fenton Karma three variable model exhibiting normal propagation.

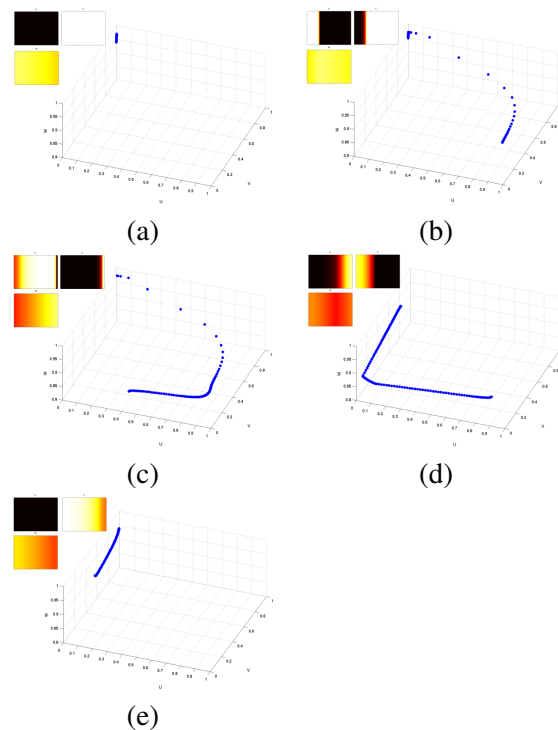


**Figure 5:** A phase space plot of the 3 parameters from a 2D Fenton Karma three variable model, showing the normal propagation of a wave of action potential at various intervals. The insets show the false colour images of the three variables. (a) rest state – the points occupy  $[U = 0, V = 1, W = 1]$ , (b) 30 ms after wave initiation along the left edge of the medium, (c) 90 ms, (d) 150 ms, (e) 210 ms.

In Figure 5 the inherent structure is clearly visible as a ‘snake’ traversing a circuit in phase

space. While this ‘snake’ is entirely expected – it occurs as cells depolarise then recover – it nevertheless provides an interesting view on wavefront propagation, and should be present even in higher variate models.

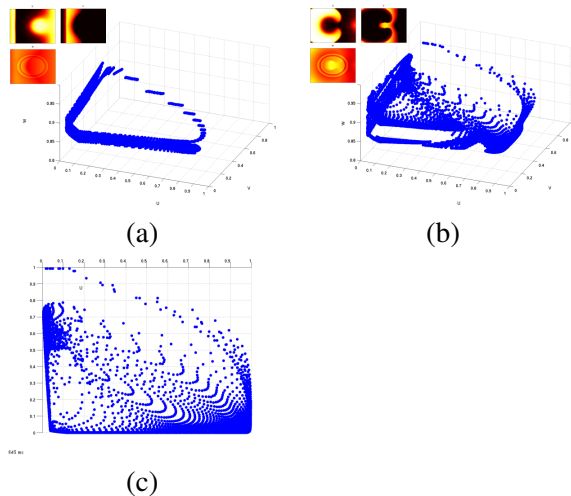


**Figure 6: A phase space plot of the 3 parameters from a 2D Fenton Karma three variable model, showing re-entrant behaviour. (a) The initiation of the second stimulus — the stimulus that causes re-entry. (b) 145 ms later, when re-entry is well established. (c) A plan view of (b).**

Perhaps more interesting effects are observed when re-entry is induced in the model. As Figures 6 (b) and (c) shows, the points that previously followed a nominal circumference have now collapsed to almost entirely fill the enclosed space.

Even this simple phase space ‘snake’ provides a novel view of the structure of the model, particularly when re-entrant behaviour is starting or stopping, and it should be useful with higher-variate models through judicious choice of the subset of variables plotted. It should be noted that adjacent points in real space can be joined in phase space, but we found this cluttered the images without providing any further insight — an intuitive ‘join-the-dots’ interpretation being the correct one.

Clearly the phase space is trivial to visualize with two or three variables, but in the case of the Luo Rudy 2 model, with 14 variables, this approach is non-trivial. If the dimension-

ality reduction techniques from section 2 reduced the phase space even by a factor of three, there would still be too many variables to visualize directly. One approach is to create multiple phase space plots, which has the advantage that all the data are shown, but the disadvantages of still having to visually combine many data sources (see Figure 8, for example). The phase space plots also have the disadvantage of removing spatial information from the visualization.

One way forward is to form visualizations based on the density and/or location of the points in the phase space, through ‘hyper-histogram’s [5], but we found this to be a less promising approach than using the propagation-model described in this paper.

## 4 Propagation-Model Based Visualization

The phase space ‘snake’ provides an expected behaviour of normal propagation, which in turn suggests the possibility of measuring the deviation from this behaviour. A number of metrics are possible for measuring this deviation — in this study we normalised the output from the simulation so that the range of each state variable was  $[0 - 1]$ , and then measured deviation as the Euclidean distance to the nearest point in the model. Ideally, the deviation would be measured as the distance from where the simulation point *ought* to be, but once re-entry is established the concept of the expected state for any given cell becomes meaningless. The nearest ‘normal’ point acts rather as an approximation to where the point would be if all were normal.

The model of normal propagation was built by capturing every point in  $n$ -dimensional phase space for a heart model simulation displaying normal action potential propagation from one edge of the domain to the opposite, for three stimuli. This model was then decimated in phase space to reduce the size of the model from several million points to a few hundred points. This decimation was motivated by two factors; firstly a large number of the points in the model were co-located

in phase-space, at least in part due to the deterministic and quantised simulations being used. Secondly, the computational overhead of performing several hundred thousand distance calculations for every node of the simulation at every point in time would be prohibitive.

The decimation was carried about by iteratively combining all model points within a radius  $\rho$  of one another into a single point at the mean location of all those points.  $\rho$  was chosen empirically to be the largest value that visually captured, in phase space, the essence of the model. Note that in this application it is not desirable to decimate by phase-space density, as the model is trying to capture a path through space, not a relative expectation of position in phase-space.

Figure 7 shows the complete and decimated models of normal propagation for the Fenton Karma three variable simulation.  $\rho$  was 0.02, which reduced the model from 5.4 million points to 528 points. Clearly the decimated model fails to capture the entire region of ‘valid’ phase space; but the essence is captured, and we found the results with this model to be insightful, as described in Section 5.1.

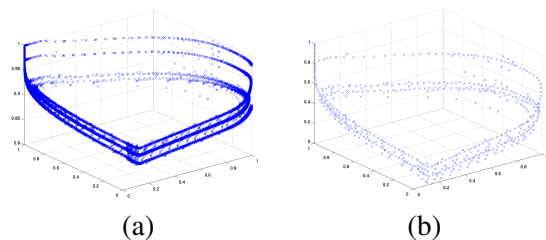


**Figure 7: The model of normal propagation for a Fenton Karma three variable simulation. (a) The full model, and (b) the decimated model capturing the essence of figure (a).**

The same process was used for the Luo Rudy 2 simulation, except that a radius of 0.01 was used, resulting in a model of 831 points. The model is partially shown in Figure 8, which displays the model by projecting it onto each of 13 axes formed by the action potential and every other state variable. Note that this figure offers some support for the existence of the phase space ‘snake’ in higher vari-

ate models.

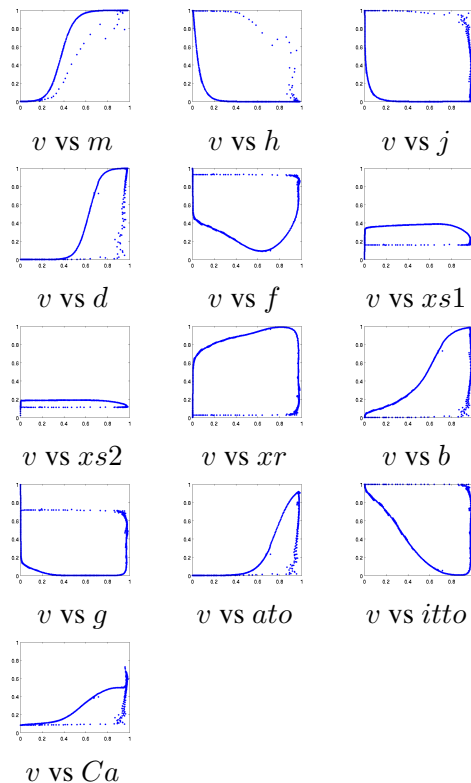


**Figure 8: The model of normal propagation for a Luo Rudy 2 fourteen variable simulation. Only a small subset of the model is shown, by plotting the action potential pairwise with every other state variable. The action potential ( $v$ ) is on the x-axis in every subplot.**

Each data point of CVT is assigned a value based on its Euclidean distance from the nearest point of the propagation model. The resulting scalar values, in the range  $[0 - \sqrt{n}]$  for an  $n$ -dimensional model, can be used, at least in this 2-D case to generate false colour images using a standard colourmap.

## 5 Results and Discussion

As expected, the visualizations of normal propagations were nearly uniform images of black, as all the distances were around zero. This can be seen in Figure 9. The small deviations from zero were due to the decimation process introducing errors.

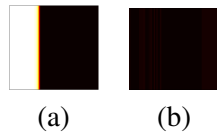


**Figure 9: The visualization of the deviation from the model of normal propagation for a normal propagation in the Fenton Karma three variable simulation. (a) The action potential output, and (b) the deviation from the model.**

As re-entry was introduced in the models, the deviations from the model grew larger, and more interesting images resulted.

### 5.1 Fenton Karma three variable

Re-entrant behaviour was introduced in the Fenton Karma three variable simulation by changing the tissue type in the central region such that the recovery following an excitation was delayed. In this way spiral waves are initiated when two stimuli are applied in close succession. The onset of re-entry is shown in the sequence of images shown in Figure 10, which are images of the action potential and the deviation from the model at 10 ms intervals,

The first feature to note in Figure 10 is that, even when re-entry is well established, nearly all the tissue in the simulation is operating within the expected model for normal propagation, that is it appears dark. The tissue that is deviating from the normal model is very clear at the leading edge of waves of propagation. This is the tissue that has not yet fully recovered from an early excitation, and is therefore inhibiting or slowing the propagation of the current excitation. This suggests the combining of the three state variables into a single image is providing an insight into the entire state of the model, in that it becomes possible to predict how the action-potential will propagate in the immediate future — something that is not easily assessed from the action-potential images alone. The second feature that can be seen on close inspection of Figure 10 is that the circular heterogeneity in the centre of the domain has become visible in this visualization, whereas it can not be seen in action potential

images alone.

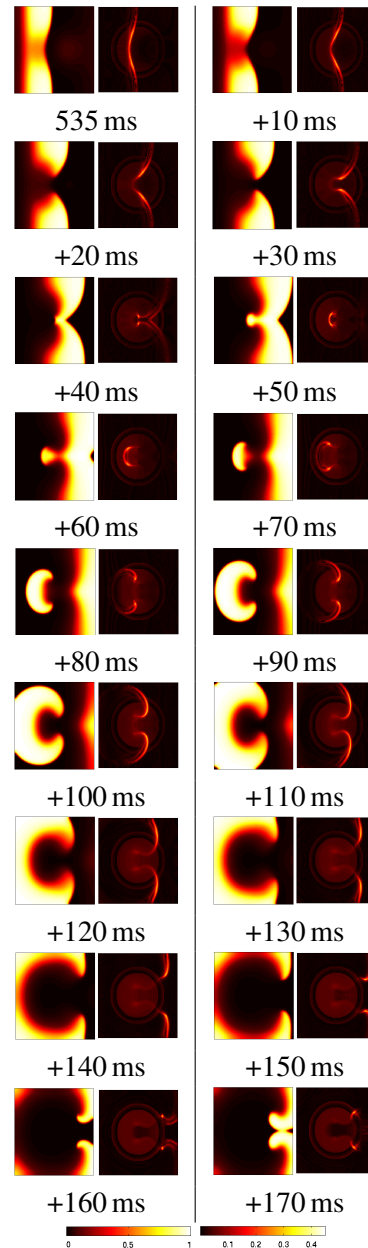


**Figure 10: The visualization of the deviation from the model of normal propagation for re-entrant behaviour in the Fenton Karma three variable simulation. The pairs of images show the initiation of re-entry following an early stimulus. The left hand image of each pair is the action potential, and the right-hand the deviation from the model. The colour-bars, shown at the bottom, correspond to the action potential images (left), and the deviation images (right).**

## 5.2 Luo Rudy 2 fourteen variable

Re-entrant behaviour was introduced in a different way for the Luo Rudy 2 simulation — instead of using heterogeneous tissue, the simulation was started in an initial condition where a re-entrant spiral wave immediately forms and continues. The formation of the wave from this artificial start condition was not of interest, so the visualizations were only generated after a settling down period. Figure 11 shows snapshots at 10 ms intervals of a single revolution of the re-entrant wave, with the action potential and the deviation from the model being displayed as before.

The features of this visualization observed in the previous section are present here, in that the re-entrant wavefront shows the largest deviation from normal, and in particular the tip of the spiral wave. This again represents the regions where propagation is being blocked or delayed. It is interesting to note the very slow drop off of this deviation behind the wavefront — behaviour which contrasts with the very sharp drop-off on the Fenton Karma simulation. This may be due a failure of the propagation model to capture normal behaviour, or that this form of re-entry genuinely does differ to this extent from normal propagation. In case, the deviation from the model seems to be far less specific than for the Fenton Karma model.

In these visualizations, the deviation from the model gives a very good impression of the excitation state of any given region of tissue; so much so the action-potential images are not really required in this figure.

## 6 Conclusions and Future Work

This paper has presented a novel method of visualizing cardiac virtual tissues, through the generation of a model of normal propagation in phase space, and measuring the deviation from this model. In the resulting visualizations, regions of CVT where the propagation of action potential is being delayed are highlighted. When combined with the visualization of ac-

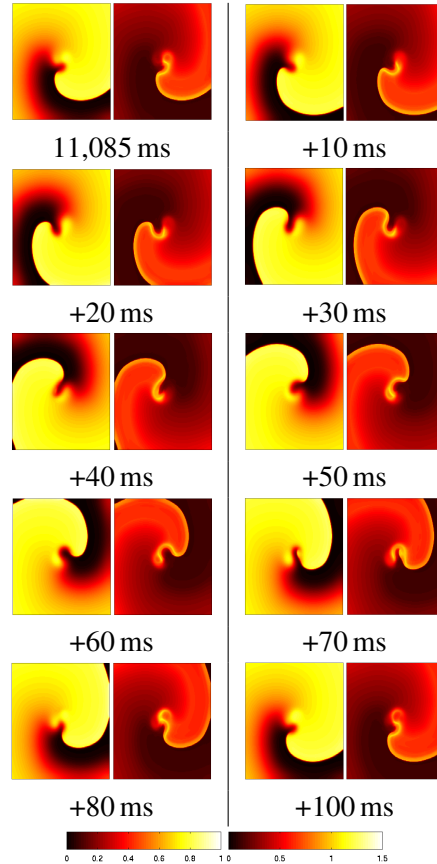


**Figure 11: The visualization of the deviation from the model of normal propagation for re-entrant behaviour in the Luo Rudy 2 simulation. The images show a complete revolution of the single spiral wave, with the action potential on the left, and the deviation from the model on the right. The colour-bars are shown at the bottom, with the left colour-bar corresponding to the action potential images, and the right colour-bar to the deviation images.**

tion potential, this provides insight into how the action potential will propagate through the tissue.

The method for calculating the deviation from the model has scope for further investigation. For instance, it might be possible to calculate the trajectory of a point in phase space during re-entry, and find the nearest model point along this trajectory (either forwards or backwards). There is also further work required on issue of normalisation — for instance is a simple intra-variate normali-



sation technique appropriate. There may also be scope in normalising the results between simulations, in that the range of possible distances increases with increasing numbers of state variables.

This visualization technique can be extended to three-dimensional simulations fairly easily. The distance metric is dimension independent, as it is based in phase space. The significant distances occur at the wave-front of action potential, so an interesting visualization might be to form an iso-surface of action potential, and colour it according to the deviation from the model.

## Acknowledgements

The authors wish to acknowledge the support provided by the funders of the UK e-Science Integrative Biology Project: The EPSRC (ref no: GR/S72023/01) and IBM.

## References

- [1] R.H. Clayton. Computational models of normal and abnormal action potential propagation in cardiac tissue: Linking experimental and clinical cardiology. *Phys. Meas.*, 22:R15–R34, 2001.
- [2] R.H. Clayton and A.V. Holden. Filament behaviour in a computational model of ventricular fibrillation in the canine heart. *IEEE Trans. Biomed Eng.*, 51:28–34, 2004.
- [3] R.H. Clayton and A.V. Holden. Propagation of normal beats and re-entry in a computational model of ventricular cardiac tissue with regional differences in action potential shape and duration. *Progress in Biophysics and Molecular Biology*, 85:473–499, 2004.
- [4] F.H. Fenton, E.M. Cherry, H.M. Hastings, and S.J. Evans. Multiple mechanisms of spiral wave breakup in a model of cardiac electrical activity. *Chaos*, 12:852–892, 2002.
- [5] J.W. Handley, K.W. Brodlie, and R.H. Clayton. Multi-variate visualization of cardiac virtual tissue. In *Proc. 19th IEEE International Symposium on Computer Based Medical Systems*. IEEE Computer Society, 2006. *In press*.
- [6] D. Noble and Y. Rudy. Models of cardiac ventricular action potentials: Iterative interactions between experiment and simulation. *Philos. Trans. R. Soc. Lond. Ser. A-Math. Phys. Eng. Sci.*, 359:1127–1142, 2001.
- [7] A.V. Panfilov and A.M. Pertsov. Ventricular fibrillation: Evolution of the multiple-wavelet hypothesis. *Philos. Trans. R. Soc. Lond. Ser. A-Math. Phys. Eng. Sci.*, 359:1315–1325, 2001.
- [8] Blanca Rodríguez, Brock M. Tice, James C. Eason, Felipe Aguel, Jr. Jos M. Ferrero, and Natalia Trayanova. Effect of acute global ischemia on the upper limit of vulnerability: a simulation study. *Am. J. Physiol. Heart. Circ. Physiol.*, 286(6):H2078–H2088, 2004.
- [9] P. Wong and R. Bergeron. 30 years of multidimensional multivariate visualization. In Gregory M. Nielson, Hans Hagan, and Heinrich Muller, editors, *Scientific Visualization - Overviews, Methodologies and Techniques.*, pages 3–33, Los Alamitos, CA., 1997. IEEE Computer Society Press.
- [10] Fagen Xie, Zhilin Qu, Junzhong Yang, Ali Baher, James N. Weiss, and Alan Garfinkel. A simulation study of the effects of cardiac anatomy in ventricular fibrillation. *Journal of Clinical Investigation*, 113:686–693, 2004.